

New Insights on the High Reconnection Rate and the Diminishment of Ion Outflow

Cheng-Yu Fan¹, Shan Wang^{1*}, Xu-Zhi Zhou¹, San Lu², Quanming Lu², Prayash Sharma Pyakurel³, Qiugang Zong^{1, 4}, Zhi-Yang Liu⁵

¹Institute of Space Physics and Applied Technology, Peking University, Beijing 100871, China

²School of Earth and Space Sciences, University of Science and Technology of China, Hefei 230026, China

³Space Sciences Laboratory, University of California, Berkeley, CA 94720, USA

⁴State Key Laboratory of Lunar and Planetary Sciences, Macau University of Science and Technology, Macau 999078, China

⁵Institut de Recherche en Astrophysique et Planétologie, CNES-CNRS, Université Toulouse III, Paul Sabatier, Toulouse 31028, France

*Corresponding author: Shan Wang (coralwang90@gmail.com)

Key Points:

- The reconnection rate normalized by ion parameters (R_i) can reach high values, attributed to insufficient field line bending outside of EDR
- Reconnection without ion bulk outflows occurs with high β_i , as the bulk represents a near-zero average acceleration across the ρ_i scale exceeding the system size
- The rate normalized to electron parameters at ~ 0.1 indicates a well-developed EDR; a high R_i indicates high absolute reconnection efficiency and weak ion coupling

Abstract

The recently discovered electron-only reconnection has drawn great interests due to abnormal features like lack of ion outflows and high reconnection rates. Using particle-in-cell simulations, we investigate their physical mechanisms. The reconnection rate, when normalized by ion parameters (R_i), may appear anomalously high, whereas that normalized by electron parameters (R_e) remains ~ 0.1 . We propose that the essence of high R_i is insufficient field line bending outside the electron diffusion region, indicating an incomplete development of the ion diffusion region. It may result from bursty reconnection in thin current sheets, or small system sizes. The ion outflow diminishes at high β_i when the gyroradius (ρ_i) exceeds the system size. Low-velocity ions still experience notable acceleration from Hall fields. However, a local distribution includes many high-velocity ions that experience random accelerations from different electric fields across ρ_i , resulting in near-zero bulk velocities. Our study helps understand reconnection structures and the underlying physics for transitions between different regimes.

Plain Language Summary

Magnetic reconnection is a fundamental energy release process in plasmas. In reconnection, both ions and electrons couple to the process, receiving energizations. The reconnection rate measures the efficiency of particle acceleration and magnetic flux transfer. However, a new type of electron-only reconnection has been observed recently, where ions do not exhibit accelerations of bulk flows, yet a higher reconnection rate compared to ion-coupled reconnections is detected. We use particle-in-cell simulations to examine the controlling factors and physical meanings of the high reconnection rate and explore the reasons for the minimal ion acceleration. We find that the high reconnection rate indicates an incomplete development of ion diffusion regions with insufficient magnetic field bending, and the minimal ion bulk acceleration is due to the average over large-scale ion gyromotion covering different fields.

1 Introduction

Magnetic reconnection is a fundamental process in plasma physics that rearranges the topology of magnetic field lines and drives many explosive energy transferring processes in space (Birn & Priest, 2007; Yamada et al., 2010). The standard model of reconnection (Figure 1a) describes a small electron scale electron diffusion region (EDR) embedded in a large ion scale ion diffusion region (IDR). On larger scales, both ions and electrons are frozen-in with the magnetic field, but they decouple from the magnetic field within the IDR and EDR, respectively.

Recently, Phan et al. (2018) reported the electron-only reconnection in Earth's turbulent magnetosheath, where no ion-scale current sheet or ion outflow is observed throughout the reconnection process. Simulation studies provided explanations of generating electron-only reconnection by either small system sizes (e.g., smaller than $10 d_i$, where d_i is the ion inertia length) as in a turbulent environment (e.g., Pyakurel et al., 2019) or a transient early phase of standard reconnection as in studies of magnetotail current sheets (Lu et al., 2020, 2022).

The reconnection rate measures the efficiency of particle acceleration and magnetic flux transferred during reconnection. It can be normalized by ion parameters (R_i) or electron parameters (R_e), both exhibiting a typical value of about 0.1 (Liu et al., 2022). However, observations show E_{\parallel} much larger than the expected value if normalized to ion parameters (on the order of 50) in electron-only reconnection (e.g., Phan et al., 2018; Bessho et al., 2022). This suggests a potentially large reconnection rate, although additional local physical mechanisms may play a role. Similarly, kinetic simulations have found high R_i in electron-only reconnections. One currently accepted controlling factor is the small system size, which gives high R_i and suppresses the ion outflow at the same time (Pyakurel et al., 2019). However, in simulation practices, the reconnection rate may be influenced by multiple parameters. Could any other factors also contribute to a high R_i ? For example, the initial current sheet thickness may be a promising candidate, as demonstrated in a contemporary study by Guan et al. (2023). Furthermore, what is the essential mechanism for high R_i ? In this study, we further examine the effects of system size and initial current sheet thickness on the reconnection rate, and try to further figure out the underlying physical meanings behind.

The ion dynamics in electron-only reconnection is also an intriguing problem. Phan et al. (2018) suggested that the limited space and/or time in the turbulent environments prevents ions from coupling to the magnetic structures. Simulations by Pyakurel et al. (2019) supported these findings, and they identified a system size of $10d_i$ as a critical transition point. Further research by Guan et al. (2023) revealed the transition threshold as ρ_i (ion thermal gyro-radius). Despite these advances, there has yet to be a detailed investigation into the exact mechanisms to explain why ions fail to experience acceleration.

In this paper, we use particle-in-cell (PIC) simulations to explore the controlling factors and physical meanings of high reconnection rates. Additionally, we investigate the behaviour of ions in simulations with and without bulk outflows to understand why ion outflows may be failed to form.

2 Simulation Setup

We conducted twelve 2.5-dimensional PIC simulations described in Table 1 using the VPIC code (Bowers et al., 2008). The x boundaries are periodic, while the z boundaries are reflecting for particles and conducting for the fields. The simulations are initialized with force-

free current sheets, where all initial currents are carried only by electrons. The guide field B_g is equal to the upstream asymptotic field B_{x0} , and $B_0 = \sqrt{B_{x0}^2 + B_g^2}$. The initial magnetic field is given by $B_x = B_{x0}[\tanh(z/L)]$ and $B_y = \sqrt{B_0^2 - B_x^2}$, where L is the half thickness of the current sheet. Reconnection occurs spontaneously from numerical noises.

In Table 1, $\frac{m_i}{m_e}$ is the ion-to-electron mass ratio, β_i (β_e) is the ion (electron) beta based on the uniform initial number density n_0 , temperature T_{i0} (T_{e0}) and magnetic field B_0 . ω_{pe} is the electron plasma frequency based on n_0 , and ω_{ce} is the electron cyclotron frequency based on B_0 . The number of particles per cell per species (nppc) is 500 in all simulations. Unless otherwise noted, the length is normalized to the ion initial length d_i (based on n_0), the magnetic field is in B_{x0} , the velocity is in $V_A = \frac{B_{x0}}{\sqrt{\mu_0 m_i}}$, and the electric field is in $B_{x0} V_A$.

The simulations are categorized into three groups. In the A and B groups, we observed the reconnection rate influenced by L and L_z , respectively, where L_z is the system size along z . In the C group, we altered T_i , and hence ρ_i and β_i , to study its effect on the ion outflow.

To simulate the realistic boundary conditions, we performed three different simulation models. ‘‘1CS’’ refers to one initial current sheet. ‘‘3CS’’ represents three initial current sheets along z of the equal thickness, with the initial currents oriented in opposite y directions for the adjacent current sheets. L_z represents the system size along z for each current sheet, so the simulation size along z in the 3CS model is $3L_z$. ‘‘1+2CS’’ means one thin initial current sheet in the middle, with two thick initial current sheets ($L = 0.5d_i$) positioned above and below. In the 1+2CS model, L_z is defined by the distance between the extreme points of B_x . The thick current sheets, which do not reconnect during the time of interest, act as realistic boundaries. Thus, particles can be constrained in the z direction through the electromagnetic force instead of by artificial reflections at the boundaries. Therefore, in group C when focusing on the ion dynamics in a small system size, the 1+2CS model is applied to completely avoid the effect of artificial boundary conditions.

3 High reconnection rate (R_i) caused by insufficient magnetic field line bending

We first study the reconnection rate. Based on the diagram in Figure 1a, the normalized reconnection rates can be written as

$$R_i = \frac{\frac{dA_y}{dt}}{B_{x0} V_{Ai}}, \quad R_e = \frac{\frac{dA_y}{dt}}{B_{xe} V_{Ae}} \quad (1)$$

Where A_y is the y component of the magnetic vector potential. The simulations do not develop or have not yet developed well-defined IDRs for the intervals of interest, so we calculate R_i using B_{x0} at the system boundaries. B_{xe} marks B_x at the EDR boundaries, defined by the edge of the central J_{ey} current layer. An additional J_{ey} layer may develop outside the central EDR with an opposite sign, partly due to the Hall effect. Thus, we choose a practical criterion for the EDR boundary at $J_{ey} = \frac{1}{10}(J_{ey,max} + 9J_{ey,min})$, which gives reasonable and consistent results throughout the reconnection development in all runs.

With simulations in group A, we examine the effect of the initial current sheet half thickness (L). The reconnection rates at the time of peak R_i are presented in Figure 1b. As L decreases, R_i increases and becomes abnormally high (approximately 0.9). Such an increasing trend of R_i with decreasing L is consistent with the contemporary study (Guan et al., 2023). In contrast, R_e remains around 0.1. Let us compare the time history of reconnection rates in runs A1 ($L = 0.03 d_i$, Figure 1c) and A5 ($L = 0.3 d_i$, Figure 1d). In Figure 1c, R_i (black line) rapidly reaches a high peak during the initial phase ($t\omega_{ci} = 0.2$ to 0.8) before dropping to a steady phase, while R_e remains consistently around 0.1 throughout the entire process. In Figure 1d, R_i and R_e both slowly rise to a steady value around 0.1, in accordance with the standard reconnection model.

In all of our simulations, R_e remains perfectly around 0.1, so we examine the abnormally high R_i by comparing it to R_e . The ratio between the two is

$$\frac{R_i}{R_e} = \frac{V_{Ae} B_{xe}}{V_{Ai} B_{x0}} = \sqrt{\frac{m_i}{m_e}} \left(\frac{B_{xe}}{B_{x0}} \right)^2 \quad (2)$$

This relationship shows that the high R_i comes from a high $\frac{B_{xe}}{B_{x0}}$ ratio. Since B_{xe} can normalize R_e effectively, the high $\frac{B_{xe}}{B_{x0}}$ ratio results from a low $\Delta B_x = B_{x0} - B_{xe}$, the magnetic field depletion outside of the EDR as illustrated in Figure 1a.

By applying Ampère's Law in the $x - z$ plane,

$$(\nabla \times B)_y = \mu_0 J_y \quad (3)$$

We take a cut at the x location of the X-line and integrate along z to obtain

$$\Delta B_x = \int_{-\infty}^{EDR} \left(\mu_0 J_y + \frac{\partial B_z}{\partial x} \right) dz \quad (4)$$

The integrals $\int_{-\infty}^{EDR} \mu_0 J_y dz$ (black) and $\int_{-\infty}^{EDR} \frac{\partial B_z}{\partial x} dz$ (green) are presented in Figures 1e and 1f, respectively. In all of our simulations, the contribution from $\int_{-\infty}^{EDR} \mu_0 J_y dz$ is an order of magnitude smaller than that from $\int_{-\infty}^{EDR} \frac{\partial B_z}{\partial x} dz$. This phenomenon can be attributed to the fact that the J_{ey} (blue) with an opposite sign from that in the central EDR, partly resulting from the Hall effect, always offsets J_{iy} (red) that arises from the ion acceleration by the reconnection electric field E_y . Consequently, it can be approximated that

$$\Delta B_x \approx \int_{-\infty}^{EDR} \frac{\partial B_z}{\partial x} dz \quad (5)$$

The term $\frac{\partial B_z}{\partial x}$ physically represents the magnetic tension, and geometrically reflects the bending of magnetic field lines in the z -direction. Thus, the low ΔB_x results from a low $\frac{\partial B_z}{\partial x}$, indicating insufficient field line bending, which further leads to high R_i .

To observe how a low L contributes to insufficient field line bending, we examine the ratio $\frac{B_{xe}}{B_{x0}}$ (blue) in Figures 1c and 1d, which is the mean value of both sides of the current sheet.

Initially, $\frac{B_{xe}}{B_{x0}}$ remains approximately 1, and then enters a rapid declining phase when the reconnection starts, followed by a transition to a steady phase. A key distinction between runs A1 and A5 is the evolution speed: in run A1, R_i peaks within a short interval ($t\omega_{ci} = 0.5$), during the declining phase of $\frac{B_{xe}}{B_{x0}}$; in run A5, R_i gradually rises to its peak ($t\omega_{ci} = 24$) during the steady phase of $\frac{B_{xe}}{B_{x0}}$. Therefore, in thin current sheets, reconnection rapidly progresses with a high reconnection rate $\frac{dA_y}{dt}$, before magnetic field lines achieve sufficient bending and hence, significant ΔB_x , resulting in high R_i .

Another important factor influencing R_i is L_z . When the field line structure extends to the system boundaries, a small L_z can restrict the space available for the field lines to fully bent, resulting in higher R_i . As shown in Figure 1g for group B, both R_i (black) and $\frac{B_{xe}}{B_{x0}}$ (blue) decrease as L_z increases. It applies to both the first R_i peak during the declining phase of $\frac{B_{xe}}{B_{x0}}$ (solid curves) and the later steady phase (dashed dotted curves). The time histories of the reconnection rate and $\frac{B_{xe}}{B_{x0}}$ for group B are provided in the Supporting Information. After the initial declining phase, $\frac{B_{xe}}{B_{x0}}$ becomes steady, while R_i exhibits peaks when magnetic islands merge. The values representing the steady phase in Figure 1g are taken at the second R_i peak, which occurs as the island merges for the first time from three to two islands (not shown), and when R_e in all runs reach similar values around 0.1 (Figure S1). The field line structures of runs B1 ($L_z = 1d_i$) and B4 ($L_z = 5d_i$) at the second R_i peak are presented in Figures 1i and 1j, respectively. It is evident that run B1 exhibits less field line bending compared to run B4.

Run B5 (3CS Model) mimics a turbulence environment, where multiple current sheets interact, resulting in significant deformation of reconnection structures and a reduced lifespan of reconnections. In the early stage, reconnection develops in a similar manner with that from the 1CS model (not shown). However, Figure 1h illustrates the field line structure at $t\omega_{ci} = 3$, where the main X-line is being disrupted by adjacent current sheets. At this time, the reconnection structure cannot be clearly defined and it ceases soon afterwards. Therefore, studying the transient reconnection behavior is important for the turbulence environment, since it may not get a chance to develop into steady states.

4 The absence of ion outflow caused by high β_i

While it is generally accepted that electron-only reconnections have high reconnection rates, it is important to note that a high reconnection rate is not necessarily associated with the absence of ion outflow. As illustrated in Figures 2a and 2c, run C1 exhibits both a high R_i and a strong ion outflow.

Figures 2e-2f depict the E_x and ion outflow structures in runs C1 ($\beta_i = 0.1$) and C2 ($\beta_i = 9$). E_x as part of the Hall field arises from the decoupling between ions and electrons and is an important factor on accelerating ions towards the outflow (e.g., Aunai et al., 2011; Yamada et al., 2018). It is noteworthy that although the E_x structures in C1 and C2 are similar, and even stronger in C2, run C1 demonstrates a strong ion outflow, while run C2 is an electron-only reconnection. A contemporary study by Guan et al. (2024) also suggests that the stronger E_x

structure in electron-only reconnection arises from greater charge separation due to the absence of ion outflow.

To investigate why ions in run C2 are not fully accelerated, we collected the ion velocity data from a specified area in the outflow region, indicated by the black circles in Figures 2c and 2d. We present the reduced ion velocity distribution functions (VDFs) in the $v_x - v_z$ plane of runs C1 and C2 in Figures 2g and 2h. A key difference is the ion velocity range: most ions in run C1 have a velocity not exceeding $1V_A$, whereas ions in run C2 can reach velocities of up to $10V_A$.

We examine low-velocity and high-velocity ions separately. In run C1, the low-velocity ions include all ions; in run C2, the low-velocity ions include those with velocities less than $3v_{thi,C1} = 0.9V_A$, as indicated by the white circle in Figure 2h, where $v_{thi,C1}$ is the initial ion thermal speed in C1. The one-dimensional reduced VDF along v_x for only low-velocity ions is shown in Figure 2i, where both simulations exhibit a similar bulk velocity drift in the $-x$ direction. To gain further insights, we observe the typical trajectories of the low-velocity ions from both simulations in Figures 2j and 2k. These ions travel over a small scale near the X-line. Using the same color scale to represent the speed along track, they exhibit nearly identical behaviors. In conclusion, the low-velocity ions in both simulations experience accelerations and show little distinction.

For the high-velocity ions, which comprise the majority in run C2, we picture the typical trajectories in Figure 2l. One trajectory is colored in rainbow that represents the speed along track, while the other two are depicted in black and purple, respectively. These ions travel at high velocities across the system scale, as was also shown in Guan et al. (2023). The ions pass through the X-line region in a short time, which limits their acceleration from the electric fields that belong to the same X-line. Additionally, they experience counter-acceleration from the opposing electric field throughout the system, which offsets their velocity. Consequently, it is highly possible that a single high-velocity ion cannot accumulate significant acceleration during the entire gyromotion process.

On the other hand, when considering the bulk ion outflow, we are not observing the behavior of a single particle, but rather the average velocity of all the ions within a local area. Since these local ions come from random trajectories across the ρ_i scale, their average velocity will therefore represent the average acceleration across the ρ_i scale. Therefore, when ρ_i exceeds the system size, the bulk ion velocity reflects the average acceleration across the entire system, which is zero due to the symmetric nature of the reconnection structures.

5 Discussion

Our results have linked the high R_i to insufficient field line bending, and it suggests that R_i in such cases cannot appropriately represent the normalized reconnection rate. Comparing our study with the standard model in Figure 1a, $R_e \sim 0.1$, indicating that the reconnection structure within the EDR is already well-developed. The standard model proposes that B_{xi} can properly normalize R_i , and in Figure 1a, we expect $B_{x0} \approx B_{xi}$. When insufficient field line bending (low ΔB_x) exists between B_{xe} and B_{x0} , $B_{x0} = B_{xe} + \Delta B_x < B_{xi}$ (the expected value of B_{xi}). Consequently, B_{x0} cannot effectively normalize R_i , and R_i loses its meaning as a normalized reconnection rate. The reduction of ΔB_x in small-scale reconnection was discussed in Pyakurel et al. (2019) and Bessho et al. (2022), but here we demonstrate that ΔB_x is contributed by field line bending with little contribution from the current density (e.g.,

discussed in Pyakurel et al., 2019). The importance of field line bending in constraining $R_i \sim 0.1$ in standard reconnection was pointed out in Liu et al. (2017). We note that the field line bending outside of the IDR would lead to $B_{x0} > B_{xi}$, but using either $B_{x0} \approx B_{xi}$ or $B_{x0} > B_{xi}$ would not alter the above analysis. Thus, our study extends the picture of field line bending to inside the IDR, concluding that insufficient bending outside of the EDR still allows for $R_e \sim 0.1$ but fails to constrain R_i .

However, R_i can still be meaningful as a description of the absolute value of the reconnection rate. Given a fixed boundary condition of B_{x0} , a higher R_i means higher $\frac{dA_y}{dt} = R_i V_{Ai} B_{x0}$, i.e., more magnetic fluxes are reconnected per unit time. It serves as a useful quantity to compare the absolute reconnection rate in observation events, as long as the upstream boundary conditions can be identified.

Additionally, the high R_i can be an indicator of the extent to which the ion acceleration deviates from the standard model. Since ions decouple from the field lines inside the IDR, the motion of field lines between the EDR and IDR boundaries is primarily due to the electron motion u_{ez} , mainly guided by the $E_y \times B_x$ drift. Therefore, insufficient field line bending can be attributed to an incompletely developed E_y structure, which is a crucial factor influencing the ion acceleration within the IDR. Our simulations also show an expanding E_y structure originating from the EDR, which corresponds with a similar J_{iy} structure, and u_{ix} grows together with J_{iy} (not shown). Thus, the insufficient field line bending and the high R_i are related with weak ion acceleration and incomplete IDR development. The decreasing phase of $\frac{B_{xe}}{B_{x0}}$ can represent the evolution process of IDR.

The electron-only phase can be either temporary or throughout the entire reconnection process. In our simulations of group A, with $L_x \times L_z = 10d_i \times 5d_i$, eventually ions are coupled and R_i reaches around 0.1. Thus, the incomplete ion coupling only occurs in the early time (Lu et al., 2020, 2022; Hubbert et al., 2021). When the initial current sheet is thick, reconnection grows slowly and the reconnection rate peaks after field lines have been fully bent, so that R_i is low in the electron-only phase, such as in our run A5 and in Lu et al. (2020, 2022). However, with a thin initial current sheet, reconnection peaks before field lines are fully bent, producing a temporarily high R_i as in our run A1. In contrast, with a small system size as in our group B and those in Pyakurel et al. (2019, 2021), the field line bending is constrained by the system size and can never fully develop. Thus, R_i remains high as long as reconnection proceeds with a fast $R_e \sim 0.1$.

The lack of the ion outflow is linked to high β_i . It is consistent with the decreasing trend of the ion outflow with increasing β_i in large-scale standard reconnection (Li and Liu, 2021). Their study also found that R_i decreases with higher β_i . The reconnection rates in our two simulations in group C only exhibit a small difference, so we cannot draw a conclusion on their relation. However, Guan et al. (2023) showed with multiple simulations that in small-scale reconnection, R_i increases with higher β_i , opposite to the trend in large-scale reconnection. Our conjecture is that when the system size is smaller than IDR, as β_i rises, the expected IDR size also increases. Therefore, it amplifies the weakening effect on ion acceleration due to the small system size, leading to a higher R_i , while R_e may remain around 0.1. In large-scale reconnection, ions are magnetized once outside of the IDR, so a lower outflow at higher β_i can

be associated with a lower reconnection rate $\frac{dA_y}{dt} = E_y = V_{out}B_{out}$, where V_{out} and B_{out} represent the velocity and magnetic field around the outflow boundary of the IDR, respectively. Then both R_i and R_e would be lower. In summary, a higher β_i leads to a weaker bulk ion outflow; it reduces the normalized reconnection rate (R_i and R_e) in standard reconnection by really reducing the reconnection efficiency, while it can increase R_i (but not R_e) in small-scale reconnection by introducing insufficient field line bending and incomplete IDR structures.

6 Conclusion

In conclusion, we have examined the normalized reconnection rates and the impact of β_i on the ion outflow using 2.5 dimensional PIC simulations. Our findings indicate that while R_i may be abnormally high, R_e remains consistently around 0.1. The high R_i is attributed to insufficient field line bending outside of the EDR, which corresponds to an incompletely developed IDR. A thin initial current sheet may produce temporarily high R_i by fast reconnection development before field lines have been fully bent, while a small system size may limit the field line bending throughout the reconnection process. A high R_i is an indicator of the extent to which ion acceleration deviates from the standard model.

Previous studies associated the small system size, high R_i , and lack of ion outflow together. However, we show that while high R_i does represent weak ion coupling, it does not indicate a complete absence of the ion outflow. The ion outflow is suppressed by the combined effects of the small system size and high β_i (i.e., large IDR size), rather than by the small system size alone. Hall electric fields develop in both cases in simulation group C, and low-velocity ions exhibit similar acceleration patterns. High-velocity ions in the high- β_i run travel rapidly through the acceleration region, receiving minimal acceleration. Statistically, the local ion bulk velocity represents the average acceleration across the ρ_i scale; thus, when ρ_i exceeds the system scale, the ion outflow diminishes.

Our analysis advances the understanding of field structures of reconnection diffusion regions and the associated particle acceleration. As we identify the essence of R_i and the ion bulk outflow, our study clarifies the relationship between normalized reconnection rates, system sizes, current sheet thicknesses, and the lack of ion outflows. The transition between different regimes related to these factors is thus understandable.

Acknowledgements

The study is supported by National Natural Science Foundation of China Grants 42374188.

Open Research

The simulation data presented in this paper are available (Fan et al., 2024).

References

Aunai, N., Belmont, G., & Smets, R. (2011). Proton acceleration in antiparallel collisionless magnetic reconnection: Kinetic mechanisms behind the fluid dynamics. *Journal of Geophysical Research Atmospheres*, 116(A9), n/a. <https://doi.org/10.1029/2011ja016688>

Bessho, N., Chen, L., Stawarz, J. E., Wang, S., Hesse, M., Wilson, L. B., & Ng, J. (2022). Strong reconnection electric fields in shock-driven turbulence. *Physics of Plasmas*, 29(4). <https://doi.org/10.1063/5.0077529>

Birn, J., & Priest, E. R. (2007). *Reconnection of magnetic fields : Magnetohydrodynamics and collisionless theory and observations*. Cambridge University Press.

Bowers, K. J., Albright, B. J., Bergen, B., Yin, L., Barker, K. J., & Kerbyson, D. J. (2008). 0.374 pflop/s trillion-particle kinetic modeling of laser plasma interaction on roadrunner. In *Proceedings of the 2008 ACM/IEEE Conference on Supercomputing (pp. 63:1–63:11)*. SC '08. Piscataway, NJ, USA: IEEE Press.

Fan, C.-Y., Wang, S. et al. (2024). Dataset for New Insights on the High Reconnection Rate and the Diminishment of Ion Outflow. [Dataset]. Zenodo. [10.5281/zenodo.14175270](https://doi.org/10.5281/zenodo.14175270)

Guan, Y., Lu, Q., Lu, S., Huang, K., & Wang, R. (2023). Reconnection Rate and Transition from Ion-coupled to Electron-only Reconnection. *The Astrophysical Journal*, 958(2), 172. <https://doi.org/10.3847/1538-4357/ad05b8>

Guan, Y., Lu, Q., Lu, S., Shu, Y., & Wang, R. (2024). Role of ion Dynamics in Electron-Only Magnetic Reconnection. *Geophysical Research Letters*, 51(19). <https://doi.org/10.1029/2024gl110787>

Hubbert, M., Qi, Y., Russell, C. T., Burch, J. L., Giles, B. L., & Moore, T. E. (2021). Electron-Only Tail current sheets and their temporal evolution. *Geophysical Research Letters*, 48(5). <https://doi.org/10.1029/2020gl091364>

Li, X., & Liu, Y. (2021). The effect of thermal pressure on collisionless magnetic reconnection rate. *The Astrophysical Journal*, 912(2), 152. <https://doi.org/10.3847/1538-4357/abf48c>

Liu, Y., Cassak, P., Li, X., Hesse, M., Lin, S., & Genestreti, K. (2022). First-principles theory of the rate of magnetic reconnection in magnetospheric and solar plasmas. *Communications Physics*, 5(1). <https://doi.org/10.1038/s42005-022-00854-x>

Liu, Y., Hesse, M., Guo, F., Daughton, W., Li, H., Cassak, P. A., & Shay, M. A. (2017). Why does Steady-State Magnetic Reconnection have a Maximum Local Rate of Order 0.1? *Physical Review Letters*, 118(8). <https://doi.org/10.1103/physrevlett.118.085101>

Lu, S., Lu, Q., Wang, R., Pritchett, P. L., Hubbert, M., Qi, Y., Huang, K., Li, X., & Russell, C. T. (2022). Electron-Only reconnection as a transition from quiet current sheet to standard reconnection in Earth's magnetotail: Particle-In-Cell simulation and application to MMS data. *Geophysical Research Letters*, 49(11). <https://doi.org/10.1029/2022gl098547>

Lu, S., Wang, R., Lu, Q., Angelopoulos, V., Nakamura, R., Artemyev, A. V., Pritchett, P. L., Liu, T. Z., Zhang, X., Baumjohann, W., Gonzalez, W., Rager, A. C., Torbert, R. B., Giles, B. L., Gershman, D. J., Russell, C. T., Strangeway, R. J., Qi, Y., Ergun, R. E., . . . Wang, S. (2020). Magnetotail reconnection onset caused by electron kinetics with a strong external driver. *Nature Communications*, 11(1). <https://doi.org/10.1038/s41467-020-18787-w>

Phan, T. D., Eastwood, J. P., Shay, M. A., Drake, J. F., Sonnerup, B. U. Ö., Fujimoto, M., Cassak, P. A., Øieroset, M., Burch, J. L., Torbert, R. B., Rager, A. C., Dorelli, J. C., Gershman, D. J., Pollock, C., Pyakurel, P. S., Haggerty, C. C., Khotyaintsev, Y., Lavraud, B., Saito, Y., . . .

Magnes, W. (2018). Electron magnetic reconnection without ion coupling in Earth's turbulent magnetosheath. *Nature*, 557(7704), 202–206. <https://doi.org/10.1038/s41586-018-0091-5>

Pyakurel, P. S., Shay, M. A., Phan, T. D., Matthaeus, W. H., Drake, J. F., TenBarge, J. M., Haggerty, C. C., Klein, K. G., Cassak, P. A., Parashar, T. N., Swisdak, M., & Chasapis, A. (2019). Transition from ion-coupled to electron-only reconnection: Basic physics and implications for plasma turbulence. *Physics of Plasmas*, 26(8). <https://doi.org/10.1063/1.5090403>

Yamada, M., Chen, L., Yoo, J., Wang, S., Fox, W., Jara-Almonte, J., Ji, H., Daughton, W., Le, A., Burch, J., Giles, B., Hesse, M., Moore, T., & Torbert, R. (2018). The two-fluid dynamics and energetics of the asymmetric magnetic reconnection in laboratory and space plasmas. *Nature Communications*, 9(1). <https://doi.org/10.1038/s41467-018-07680-2>

Yamada, M., Kulsrud, R., & Ji, H. T. (2010). Magnetic reconnection. *Reviews of Modern Physics*, 82(1), 603–664. <https://doi.org/10.1103/RevModPhys.82.603>

Table 1. Plasma parameters of twelve simulation runs

Run	$\frac{m_i}{m_e}$	ρ_i/d_i	β_i	β_e	$\frac{\omega_{pe}}{\omega_{ce}}$	L_x/d_i	L_z/d_i	L/d_i	Δ/d_i	Model
A1	100	1.58	2.5	0.5	5	10	5	0.03	0.01	1CS
A2								0.05		
A3								0.1		
A4								0.2		
A5								0.3		
B1	100	1.58	2.5	0.5	5	5	1	0.03	0.005	1CS
B2							1.5			
B3							2			
B4							5			
B5							1		0.01	
C1	900	0.32	0.1	0.2	2	1	1	0.05	0.001	1+2CS
C2		3	9							

Note: $\frac{m_i}{m_e}$: ion-to-electron mass ratio. ρ_i : ion gyroradius. β_i (β_e): ion (electron) beta. $\frac{\omega_{pe}}{\omega_{ce}}$: ratio between the electron plasma frequency and electron cyclotron frequency. L_x : system size along x. L : initial current sheet half thickness. Δ : size of one cell. Model: simulation model. See text for details.

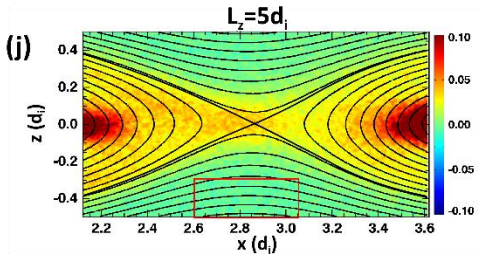
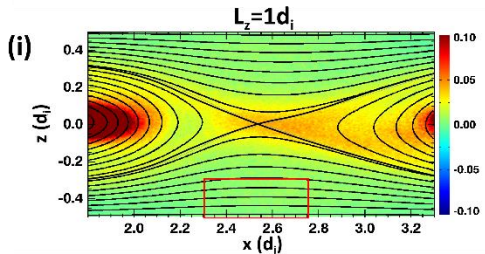
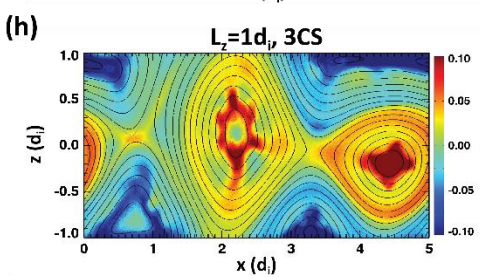
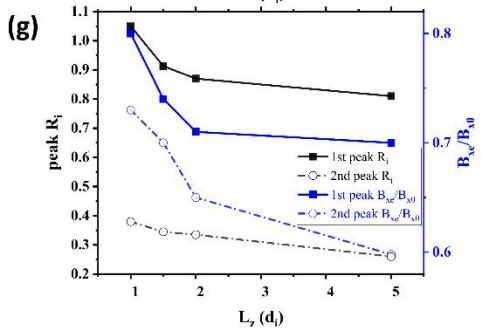
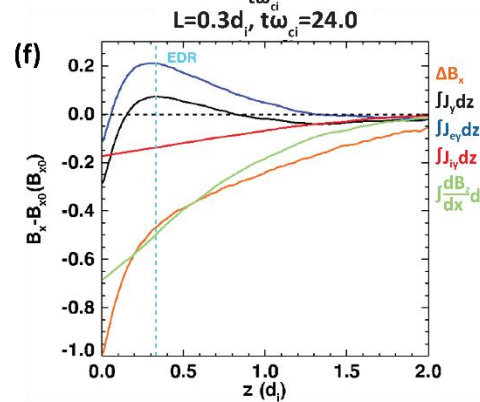
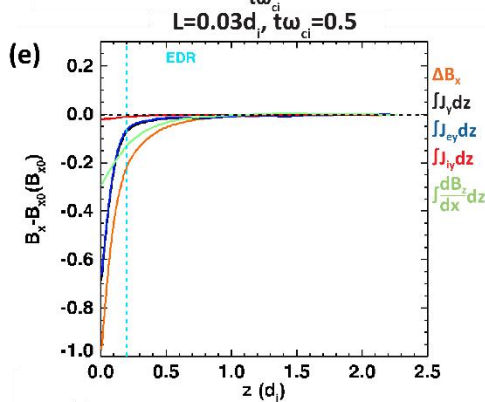
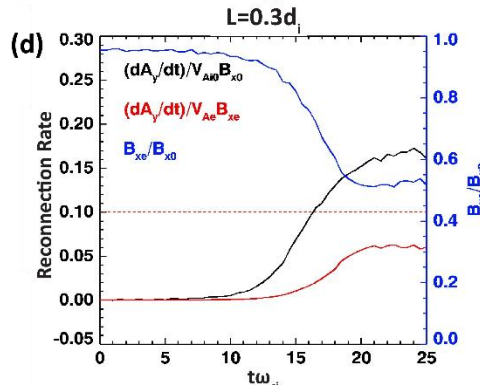
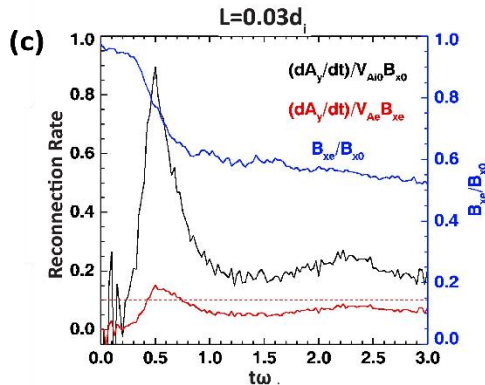
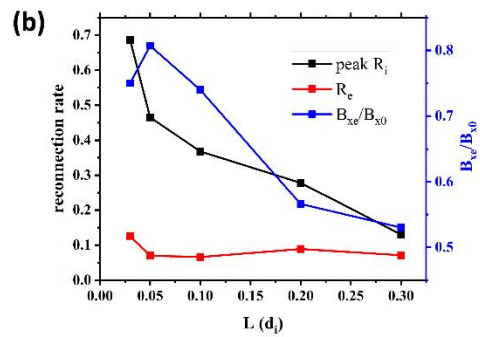
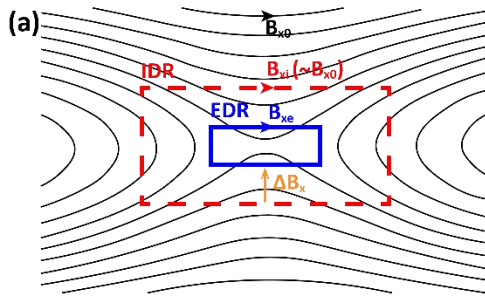


Figure 1. (a) The structure of diffusion regions. (b) to (f): Reconnection rates affected by the initial current sheet half thicknesses (L). (b) Simulation Group A: Peak R_i , R_e and $\frac{B_{xe}}{B_{x0}}$ at the time when R_i reaches the peak. As L increases, R_i and $\frac{B_{xe}}{B_{x0}}$ both decrease, while R_e always remains around 0.1. (c) and (d), runs A1 ($L = 0.03 d_i$) and A5 ($L = 0.3 d_i$): the evolution of R_i (black), R_e (red) and $\frac{B_{xe}}{B_{x0}}$ (blue) over time. In both cases, as reconnection develops, $\frac{B_{xe}}{B_{x0}}$ first decreases and then becomes stable as R_e reaches around 0.1. In run A1, reconnection develops rapidly, associated with R_i reaching a high peak; in run A5, R_i gradually increases to around 0.1. (e) and (f), runs A1 and A5: B_x (orange), the integral of j_y (black) and $\frac{dB_z}{dx}$ (green) from the upper system boundary to the upper EDR boundary along the x location of the X-line at the time when R_i peaks. ΔB_x is mainly contributed by $\frac{dB_z}{dx}$. Despite j_{iy} (red) is larger in A5, j_y remains small as j_{iy} offsets j_{ey} (blue). (g) to (j): Reconnection rates affected by the system size along z (L_z). (g) Simulation group B: R_i (black) and $\frac{B_{xe}}{B_{x0}}$ (blue) at the time when R_i reaches the first peak (solid) and the second peak (dashed dotted). As L_z decreases, R_i and $\frac{B_{xe}}{B_{x0}}$ both decrease. (h) run B5: out of plane current at $t\omega_{ci} = 3$. In turbulent environment, strong deformation is observed. (i) and (j), runs B1 ($L_z = 1d_i$) and B4 ($L_z = 5d_i$): the reconnection rate R_i at the second R_i peak. Less field line bending is observed in B1 than in B4.

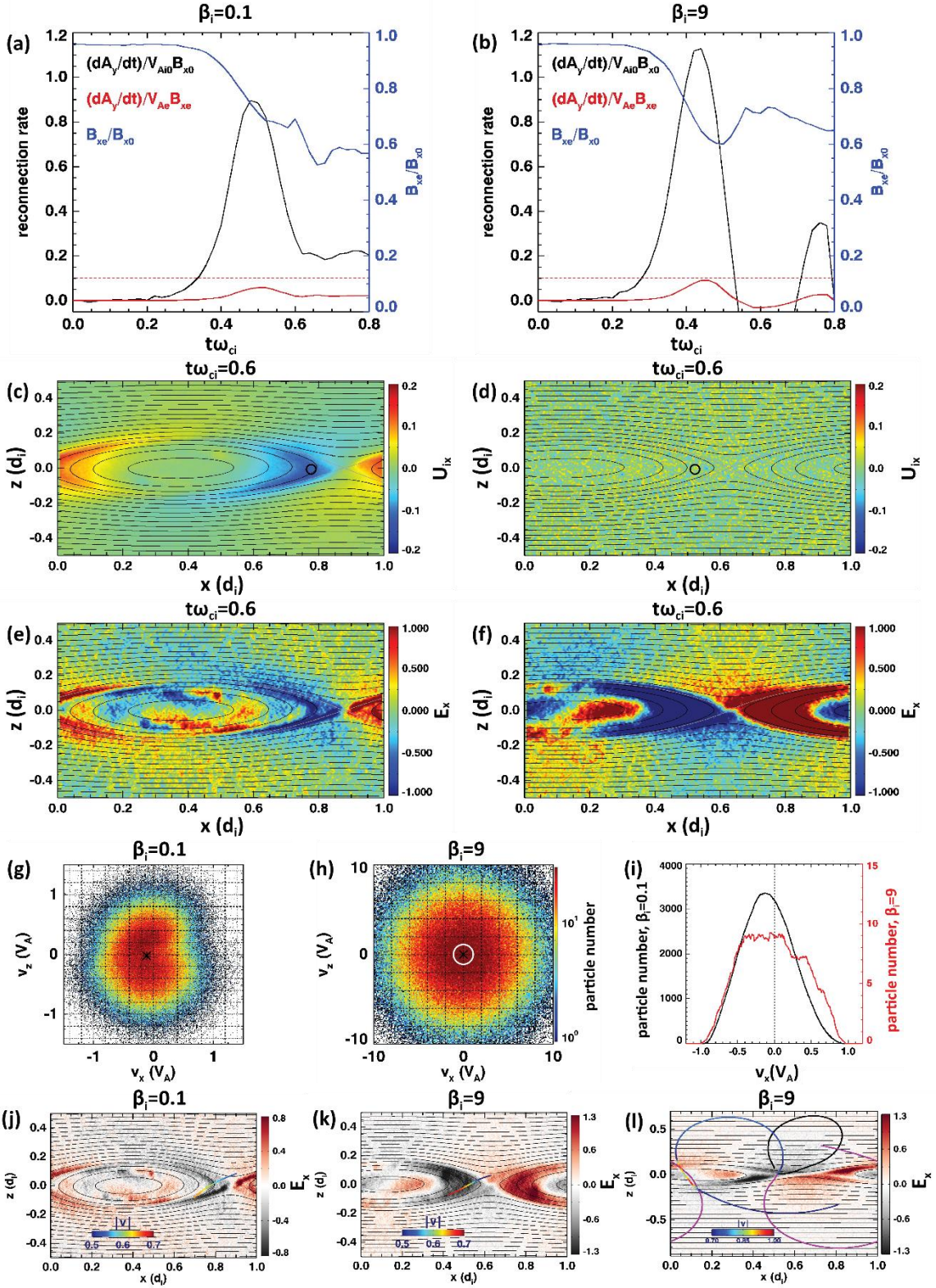


Figure 2. (a) to (f): Reconnection ion outflows affected by β_i , run C1 (left) with $\beta_i = 0.1$ and run C2 (right) with $\beta_i = 9$. (a) and (b), the evolution of R_i , R_e and $\frac{B_{xe}}{B_{x0}}$ over time. Both runs exhibit large peak R_i . (c) and (d), significant ion outflow U_{ix} observed in run C1, while no ion exhaust is present in C2. Black circles represent the outflow region where the ion velocity data were collected for the analysis. (e) and (f), similar E_x structures observed near X-line in both runs, stronger in C2. (g) to (l): Ion particle data from the outflow region of runs C1 and C2. (g) and (h), reduced ion VDF in the $v_x - v_z$ plane. (i) One-dimensional reduced ion VDF along v_x . For C2 (red), only low-velocity ions with $|v| < V_A$ (within the white circle in (h)) are collected. Distributions in both runs exhibit a bulk velocity drift in the $-x$ direction. (j) and (k), typical trajectories of ions in run C1 and low-velocity ions in Run C2 overplotted on E_x at $t\omega_{ci} = 0.6$. Colors along the trajectories represent their speeds, showing similar accelerations. (l) Typical trajectories of high-velocity ions in Run C2 overplotted on E_x at $t\omega_{ci} = 0.4$. One of the trajectories is colored in rainbow, showing little and reversing accelerations over one cyclotron period. Two additional trajectories are shown in black and purple. Since the gyroradius exceeds the system scale, ions in the local distribution experience the acceleration across the whole system, leading to a negligible bulk velocity.